Multi-step modeling of rotating gliding-arc plasma reactor applied for carbon black synthesis

Felipe Antonio Cassini[1], Deisei Rebelo Consoni[2], Leonardo Paes Rangel[3], Natan Padoin[3], Cintia Soares[3], Nito Angelo Debacher[1, *]

[1] Department of Chemistry, Universidade Federal de Santa Catarina, Brazil
[2] Department of Mechanical Engineering, Universidade Federal de Santa Catarina, Brazil
[3] Department of Chemical and Food Engineering, Universidade Federal de Santa Catarina, Brazil

* Corresponding author: nito.debacher@ufsc.br (Nito A. Debacher)

Abstract

Plasma is ionized gas produced by electric discharges and can be obtained in several different ways from different devices and can be generally separated into two main categories, namely, thermal and non-thermal plasma. At times, a combination of thermal and non-thermal plasma is desired for industrial applications such as carbon black (CB) production via propane pyrolysis, for example, and it can be achieved through a transient gliding arc discharge device. The plasma pyrolysis process is environmentally clean, as the only byproducts are H_2 gas and solid CB; however, the physical and chemical processes involved are very complex, and a computational modeling tool is essential for its optimization. This work mainly focused on developing a rotating gliding arc (RGA) plasma discharge reactor operating with alternating current high-voltage and a low current regime at atmospheric pressure for continuous CB synthesis by propane pyrolysis. The CB particle structure identified was a turbostratic type with small particles fused and graphitic layers randomly formed. The pressure and velocity profiles as well as electric field strength at the electrode area of the RGA reactor were optimized via COMSOL® Multiphysics software. The chemical composition profile of the RGA reactor in ideal working conditions was estimated via T&TWinner software based on the Gibbs free energy minimization method. The multi-step modeling calculation and the experimental results show that the rate of degradation of propane is high at the electrode tip, which shows a direct relationship with the intensity of the electric field. The multi-step modeling calculation showed to be a strong tool for an RGA reactor design for efficiency achievement.

Keywords: Rotating gliding-arc, plasma reactor, carbon black synthesis, multi-step modeling.

1. Introduction

Carbon is the most versatile element after hydrogen, forming many compounds and molecules with diverse characteristics and functions. Among various compounds on solid phases, carbon nanomaterials are useful in many applications and new technologies. Usually, carbon nanomaterials comprise carbon nanotubes, fullerenes, carbon black (CB), carbon fiber, and, recently, graphene. Carbon black (CB) has been the first carbon nanomaterial produced on an industrial scale, with an estimated world production rate of 8 million tons per year [1, 2]. CB is used in many different industrial processes, including metals and chemicals, electronics and semiconductors, aerospace, and automotive, as well as photonics and optics depending on its chemical, structure, electrical, and optical properties [3]. From a chemical viewpoint, CB manufacturing is separated into two categories, namely, incomplete combustion and thermal decomposition, both based on the reaction of a hydrocarbon feedstock. However, from an industrial viewpoint, the process of furnace black or thermal black (acetylene black) is the most used [4, 5]. In terms of quality, thermal decomposition has advantages over incomplete combustion [4, 5, 6].

Residual gases produced by an incomplete combustion process are linked to global warming and incompatible with sustainable development. Therefore, from economic and ecological viewpoints, the plasma process provides an interesting alternative CB production method. The main process with plasma is

hydrocarbon pyrolysis through an external electric power supply that sustains an electric discharge, according to the reaction, as shown in Equation 1:

$$C_nH_m \rightarrow nC + m/2H_2 \qquad\qquad (1)$$

Furthermore, plasma technology has been used as either a new alternative technology or a complement to existing technology, because of its advantages, including high energy density and temperature, higher energy efficiencies, and non-selective treatment [7, 8]. Plasmas are partially or strongly ionized gases created by electric discharges. In the pyrolysis application, the process is environmentally clean because it does not produce greenhouse gases, only H_2 and solid carbon (as seen in the reaction in Equation 1). Among different technologies used in chemical and engineering processes, plasma can be generally separated into two main categories, namely, thermal and non-thermal plasma. In thermal plasma, all constituents are characterized by thermodynamic equilibrium; for non-thermal plasma, the different constituents are not in thermodynamic equilibrium where the electron temperature is higher than neutral and ion temperatures. Both thermal and non-thermal plasma processes have been used for CB production such as direct current (DC) plasma torch [7, 9], alternating current (AC) plasma torch [2, 6], hybrid DC radio frequency plasma reactor [10], AC high-voltage plasma [11, 12], atmospheric non-thermal plasma [13], and transient gliding arc plasma reactor [1, 14]. Transient gliding arc plasma is produced by a periodic discharge from arc to transitional discharge with a high electron density level. Hence, thermal and non-thermal plasma can be combined in the same apparatus through transient gliding arc discharge mechanisms [13, 15], which allow high power (enhanced productivity) and high selectivity for the chemical reactions.

A conventional gliding arc device operates with divergent flat electrodes in a 2−D plane that lets most of the gas flowing outside of the discharge. This problem can be solved via a gliding arc regime that operates in a 3−D plane, providing a better mixture and enhancing the gas discharge contact time. With this purpose, two gliding arc reactors have been proposed, one containing a forward rotating discharge [14] and the other a reverse rotating discharge [15]. According to Zhang et al. [14], rotating gliding arc (RGA) reactors are promising design plasma devices, with the best conditions for hydrocarbon reforming and environmental protection. An RGA reactor design is a complex task since highly nonlinear phenomena occur even under optimal operational conditions. However, using computational tools can overcome these difficulties by providing information at different levels, which can be used to analyze the existing reactors' performance and design new ones. Modeling fluid dynamics within the reactor helps with finding new configurations to maximize plasma torch stability. Additionally, electrostatics analysis at the electrode region helps identify topological features that ensure high electrical field strengths and provide requirements to start and maintain the electrical arc.

A multi-step model developed with simulation software can be applied to the underlying plasma physics process to analyze optimal conditions for the RGA reactor design and operation. The computational methodology for designing RGA is based on two simulation software programs, namely, COMSOL$^©$ Multiphysics and T&TWinner [16, 17]. COMSOL$^©$ Multiphysics was applied to model fluid dynamics and electrostatics within the reactor, whereas T&TWinner was applied to model the chemical equilibrium within the reactor.

Thus, this work aimed to develop an RGA plasma discharge operating in a high-voltage and low current regime at atmospheric pressure using nitrogen-propane for continuous gas-phase CB synthesis. A multi-step model was applied with simulation software to the underlying plasma physics process to optimize the conditions for reactor design and operation. Additionally, experiments were conducted to examine the plasma gas flow rate's influence on plasma stability and the propane flow rate in the CB morphology. The CB growth mechanism was discussed based on calculations of thermodynamic equilibrium and its morphology from the experimental analysis.

2. Experimental

2.1 Materials

The propane (C_3H_8) gas used was of commercial grade (99.5%) purchased from PETROBRAS. The plasma working gas was nitrogen of commercial grade (99.5%) from White Martins$^©$.

2.2 RGA plasma reactor

The RGA plasma reactor setup and the power supply used in the continuous gas-phase CB synthesis at atmospheric pressure are shown in Fig. 1. The central electrode was a 4 mm tungsten rod containing 2% thorium, and the surrounding electrode was copper water-cooled of 7–12 mm diameter.

The copper smallest-diameter electrode provided the acceleration of the gas within the chamber cooling the central electrode. The copper largest-diameter electrode provided a gas velocity reduction due to gas expansion. The change in diameter was used to limit the arc length and to enhance the gas mixture of nitrogen and propane. The nitrogen working gas was injected through six tangential holes in the first injection chamber. The propane was injected through four holes placed slightly tangentially below the first chamber since vortex formation enables the discharge rotation within the plasma reactor. Two magnet neodymium rings were positioned axially with the electrodes to accelerate the electric arc rotation. The plasma reactor was connected to a post-discharge chamber of an insulated metal pipe of an internal diameter of 76 mm and a length of 500 mm. At the post-discharge chamber, the gas pressure falls to induce CB precipitation.

The electrical power supply used was an AC high-voltage transformer of 60 Hz, operating with a maximum voltage of 3 kV and a maximum power of 15 kW. The current was limited by a capacitor bank of 3.95 μF and an inductor with 111 mH connected in series with the secondary transformer. All these elements were applied to limit the current provided, similar to the ballast effect used in power supplies for thermal plasma [18]. The voltage and current discharge signals were measured with a Tektronix (TCP3014B) digital oscilloscope using a high-voltage probe (P6015A) and a Hall effect current probe (TCP202A) varying the nitrogen flow rate at 10, 15, 20, and 25 L·min^{-1}.
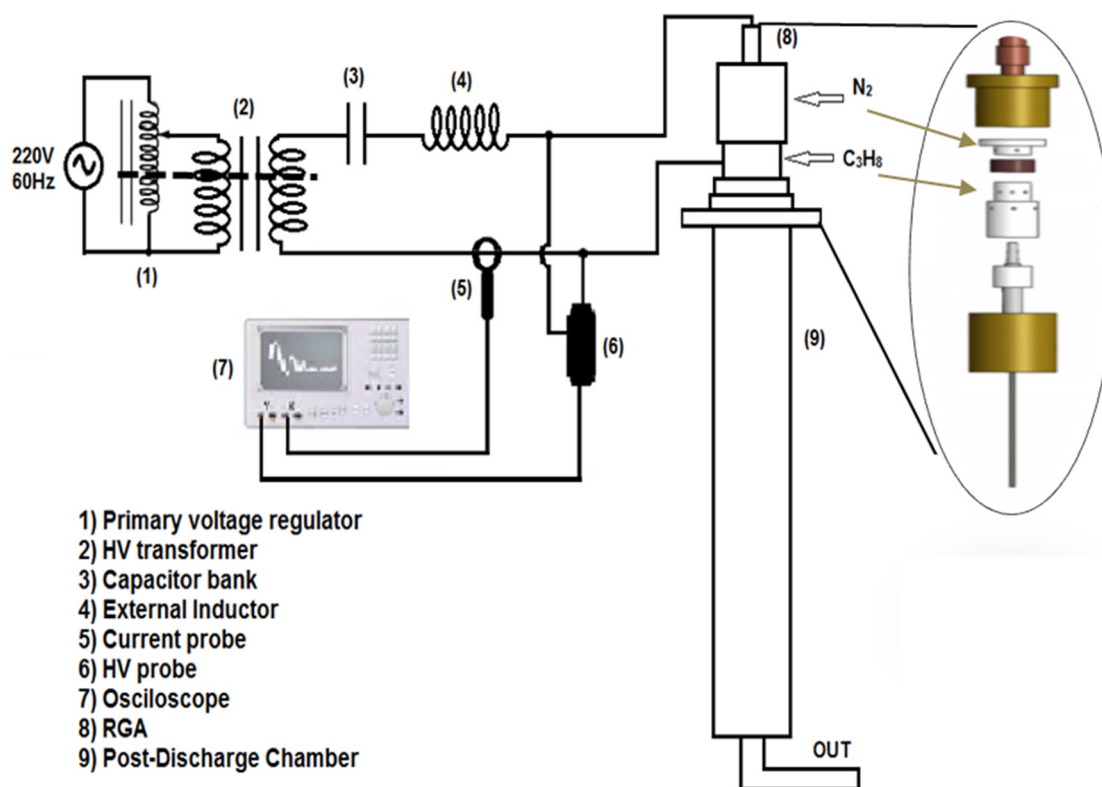

Fig.1. Schematic setup of the rotating gliding arc (RGA) plasma reactor showing the power
supply and gas inlets.

2.3 CB analysis

The CB samples' morphology was characterized using scanning electron microscopy coupled with an energy-dispersive X-ray spectroscopy (SEM-EDS, JSM-6390 LV) conducted at 20 kV. The analysis was made with and without metallization, respectively. The first analysis provided images of larger CB agglomerates. In the

second analysis, samples were sonicated in acetone and deposited over a silicon plate for the particle aggregation images.

The transmission electron microscopy (TEM) analysis of CB, the sample was sonicated in acetone and deposited on copper microgrids and coated with an amorphous carbon layer. After drying, the microgrids were analyzed by TEM at 100 kV (JEM 10110) and at 200 kV (high-resolution TEM [HRTEM], JEM2100). Selected area electron diffraction (SAED) patterns were taken on a selected circular area with a 200 nm apparent diameter enveloped a small CB particle. The particle's crystal structure analysis was recorded via X-ray diffraction (XRD, Enraf-Nonius) using a Cu–Kα radiation (λ = 1.5418 Å) in the 10° to 90° range. Raman analysis was conducted using a continuous wave laser of 514.5 nm with a Renishaw–Raman spectrometer (inVia^{TM}). The spectrum was followed in the range of 1000 to 2000 cm^{-1}.

2.4 The plasma chemical equilibrium modeling

The plasma pyrolysis chemical equilibrium composition analysis was modeled through T&TWinner software at the electrode area, which is based on the Gibbs free energy minimization method. All calculations were based on temperature and pressure input [19].

The propane pyrolysis modeling in the RGA reactor, 30 species were considered, including electrons, ions, radicals, neutral, and atomic species. All species were selected according to the literature related to the CB process and propane pyrolysis. Analysis focused on the first nuclei formation to start aggregation and agglomeration of soot, and CB growth was considered as the first approximation of the local thermodynamic equilibrium [1].

2.5 The plasma fluid dynamic modeling

The plasma fluid dynamic modeling in the RGA reactor based on a bench-scale prototype was modeling using the COMSOL$^{©}$ Multiphysics software. Navier–Stokes and mass conservation equations were solved in a 3–D computational domain, reproducing the experimental main features. Unity velocity of (m·s^{-1}) was imposed at the reactor inlet, whereas null gauge pressure was considered at the outlet. No-slip boundary condition was applied on the reactor walls, and nitrogen gas was used as the plasma working gas. The 3–D computational domain was discretized with an unstructured mesh of approximately 1.3×10^6 elements. A mesh convergence study was successfully developed to verify discretization level suitability. The fully coupled system of equations was solved iteratively through the GMRES (generalized minimal residual method) solver. Convergence was obtained when the relative errors of the numerical solution were below 10^{-3}.

2.6 The plasma electrostatic modeling

Electrostatics at the RGA reactor's electrode area were modeled in a 2–D axisymmetric computational domain for the model features highlighting the applied boundary conditions. An electric potential difference of 4.6 kV was assigned at the electrodes of tungsten and insulation by polymeric support. Furthermore, the ground condition was specified at the remaining boundaries and different electrode tip topologies were evaluated. The entire domain was discretized with an unstructured mesh comprising approximately 2.0×10^4 elements. A mesh refinement study was conducted to ensure that the results obtained were grid independent. The fully coupled system of equations was solved iteratively through the GMRES solver, and convergence was obtained when the relative errors of the numerical solution were below 10^{-3}.

3. Results and discussion

3.1 Discharge regime

For fixed electrode geometry (diameter and length), the electric discharge occurrence was observed through the cyclic gliding arc discharge. The associated AC high-voltage power supply allows discharge in both positive and negative cycles in which the current has an opposite signal from the voltage. The time evolution of discharge operating in a gliding arc regime is shown in Fig. 2 (a). During the gliding arc evolution, plasma goes through different states, and those phases are shown by red lines in Fig. 2 (b). Physical phenomena, such

as changes in the electric field current and voltage, heat transfer processes, system instabilities, temperature, and equilibrium, occur during one cycle evolution of the non-stationary electrical discharge. The mechanism behind the time evolution inside of RGA can be described as follows: point A (Fig. 2 (a)), the voltage is sufficient to cause a gas breakdown at a small distance between electrodes and the voltage falls to the lowest value. Shortly after the gas breakdown, the current reached its highest value (zone 2, Fig. 2 (b)).

Fig. 2. a) Time evolution of current–voltage rotating gliding arc (RGA) discharge. AC high-voltage transformer (capacitance C = 3.95 µF; inductor L = 111 mH; N_2 flow rate 15 L·min^{-1}). b) Scheme of gliding arc regime separated by zones of plasma discharge evolution (red lines). 1, copper electrode; 2, tungsten electrode.

As the gas blows the discharge arc increases the discharge length, the arc resistance increases along with the arc voltage (zone 1, Fig. 2 (b)) until it reached the maximum value, limited by electric source capacity. As a consequence, there is still high current which diminish when arc breaks after passing the edge of the copper electrode, and a new discharge gas rupture occurred (point B, Fig. 2 (a)) at the shortest distance between electrodes to start a new cycle (zone 2). Zero-current means the interval between two consecutive arcs, therefore, zone 1 ends at the current peak and zone 2 ends when current is zero. After the plasma torch nozzle turned off, the expansion in the post-discharge region decreases the gas temperature leading to a carbon particles' growth (zone 3, Fig. 2 (b)).

After 15 min operating times, CB deposits at the tip of the rod electrode induce a preferential path for discharge as shown in Fig. 3.

Fig. 3. Carbon black deposits on the tip of the rod electrode.

The voltage–current characteristics for the RGA are shown in Fig. 4. As shown in Fig. 4 (a) – (d), if the voltage drops as the current increases, starting from 5A, this is due to the increase in plasma conductivity by the increase in temperature. However, for further increase in current leads to higher Joule heating and decrease in plasma conductivity, forming an electric arc, changing regime from RGA to electric arc discharge plasma and at this regime, the voltage increases as the current increases [20]. As can be observed from Fig. 4 (a) – (d), the changing in the regime depends on the gas flow rate due to gas temperature and conductivity and electrode and reactor configuration.
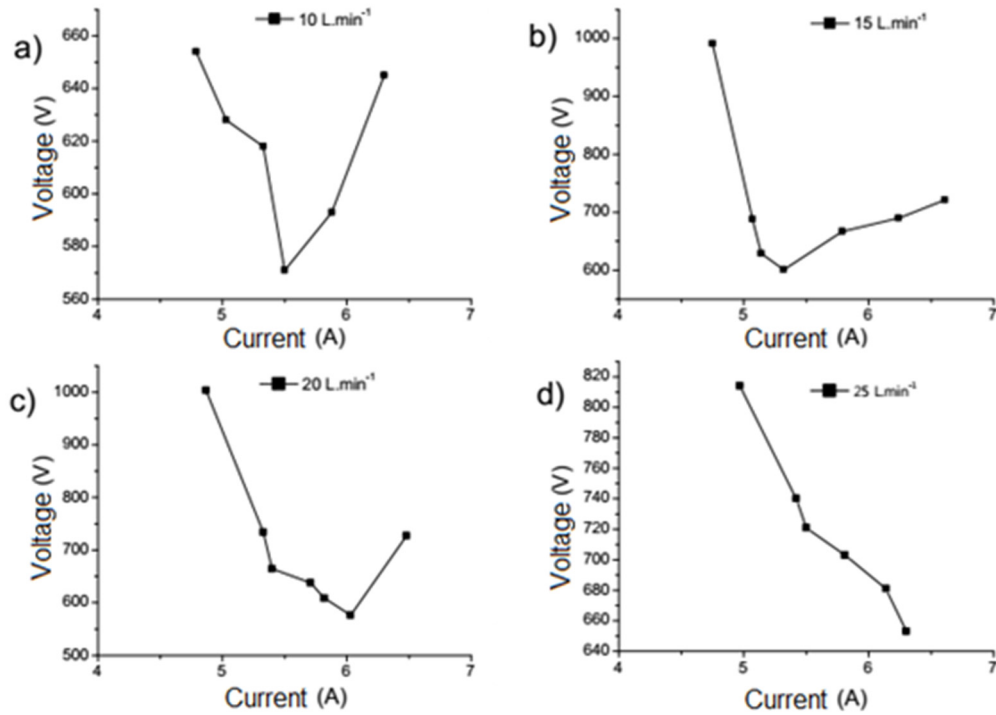
Fig. 4. Voltage–current characteristics measured for rotating gliding arc (RGA) using N_2 as plasma gas.

3.2 CB morphology

Samples A–D in Fig. 5 show larger agglomerates collected in the post-discharge chamber walls. CB surface texture is similar in all samples, exhibiting huge compact lamellas. The plasma setup conditions used are shown in Table 1 for each sample.
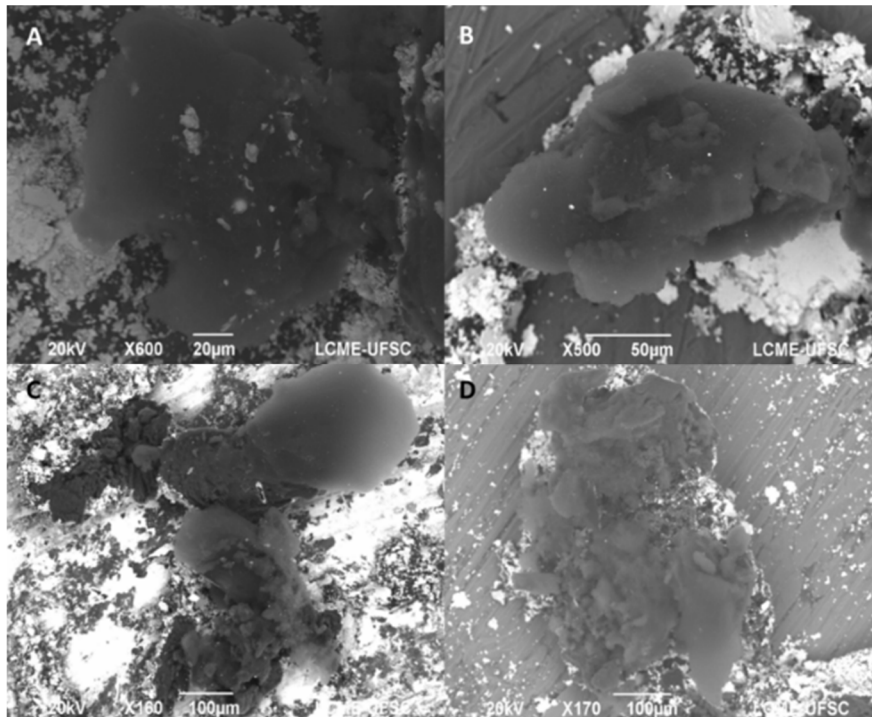

Fig. 5. SEM images of agglomerates of synthesized carbon black (CB). The samples (A–D) are on conditions as described in Table 1.

Table 1. Experimental conditions of nitrogen–propane continuous gas-phase CB synthesis.

Sample	N_2 (L·min^{-1})	C_3H_8 (L·min^{-1})
A	15	1
B	25	1
C	25	2
D	15	2

The internal morphology of CB is shown in Fig. 6. It appears in two forms: the first comprises a randomly oriented particle without a specific structure (like soot) and the second appears as many spherical particles that form aggregates (Fig. 6 (a)). The analysis made in a silicon plate provided the visualization of a small aggregate, confirming that it is formed by small spherical particles (Fig. 6 (b)). The junction of a larger quantity of these small spherical particles and randomly oriented particles form huge agglomerates that possibly grew in zone 3, as shown in Fig. 2 (b).
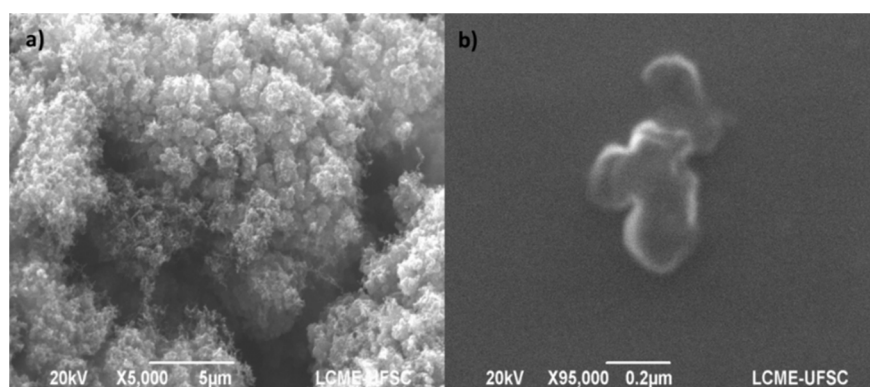

Fig. 6. a) SEM images of internal morphology analysis of carbon black (CB); b) SEM image of tiny particle aggregate obtained using a silicon plate for SEM analysis.

The energy-dispersive spectrum (EDS) from CB in sample A obtained as described in Table 1 is shown in Fig. 7. The EDS results show that the sample composition is mostly carbon element with some impurities from the copper electrode due to erosion [21].

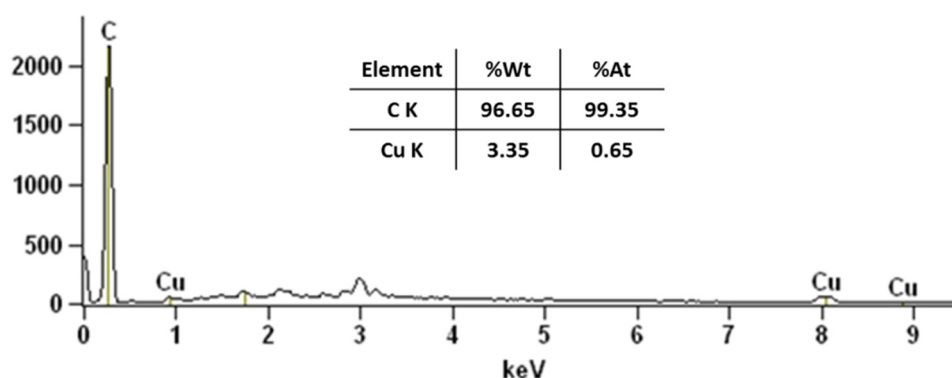| Element	%Wt	%At
C K	96.65	99.35
Cu K	3.35	0.65

Fig. 7. SEM-EDS spectrum for carbon black (CB) obtained in pyrolysis condition (sample A) as presented in Table 1.

The microstructure and nano-texture of synthesized CB are examined by using TEM images. The CB particle microstructure of two groups is presented in Fig. 8. The first comprises small particles that fuse together to form a chain or cluster of carbon particles (Fig. 8 (a)). The other part appears as graphitic layers fused and packaged randomly around a nucleus (Fig. 8 (b), (c)). These different structures are due to the CB growth process occurring in a temperature gradient within the reactor on the gliding arc regime. A single tiny particle formed by graphitic sheets, similar to a "boat" where the edges have a greater graphitization degree, is shown in Fig. 8 (d). These particles comprise a junction of these two groups to form the CB aggregates particle structure.
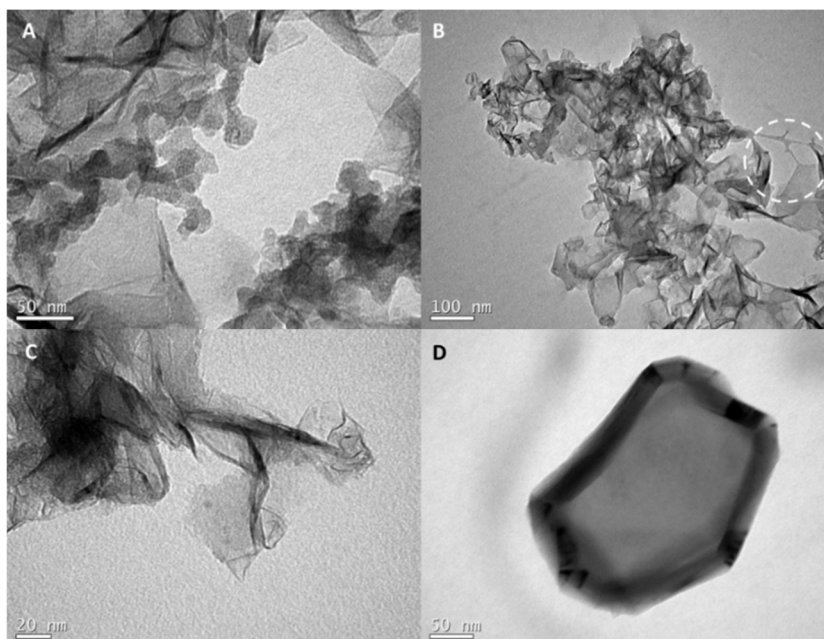
Fig. 8. TEM images obtained after propane pyrolysis using a rotating gliding arc (RGA)—
two groups of carbon black (CB). a) Small particles fused and randomly organized; b) and
c) Graphitic layers fused and packaged randomly forming an aggregate particle of carbon
black (CB); d) "Boat" shape of a carbon black (CB) particle.

SAED patterns (Fig. 9 (b)) around a tiny CB particle (Fig. 9 (a)) show weak reflection rings in *hkl* plane 002 and in *hk* planes 10 and 11 and dislocated diffraction points, thus indicating both disorder in the packaged directions and little dimensions in the related directions. A single graphite particle was considered for simulation over the SAED pattern, as shown in Fig. 9 (c). The simulated *hkl* planes reveal that the smallest basic structure forming CB aggregates are graphite microcrystals. The d_{002} mean value distance calculated is 3.557 Å, which is higher than the value reported for graphite (d_{002} = 3.354 Å).
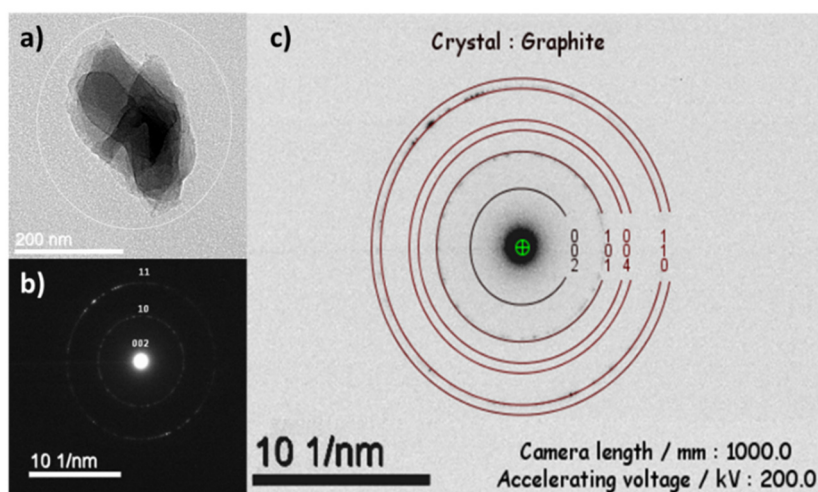

Fig. 9. a) Selected area around one particle for SAED pattern; b) SAED pattern, c) *hkl*
planes simulating a microcrystal of graphite over SAED pattern measured for carbon black
(CB).

HRTEM images (Fig. 10) show that a random stacking of carbon sheets occurs in some directions (Fig. 10 (b)) but also occurs among well-aligned carbon sheets (Fig. 10 (a)), forming microcrystals with small lengths that lose the stacking direction in a few nanometers dispersed in a carbon matrix semi-crystalline. The Bragg fringe lengths shown in Fig. 10 (a), indicated by the arrow, tend to be shorter than the graphene layers stacking, indicating a lack of coherence in stacking these layers. SAED patterns and TEM images show characteristics of turbostratic materials [1, 6, 7, 10, 12, 22, 23], where the semi-crystalline structure can be defined in terms

of hexagonal layers stacked roughly parallel to each other with random rotation and translation in the same plane, as shown in the highlighted circle in Fig. 10 (b). For this reason, many distortions and discontinuities are observed along the carbon particles' length. All samples had the same microstructure and nano-texture, differing only in soot proportion visualized in some TEM analysis, indicating that the flow of propane and nitrogen does not influence the CB structure, just in proportion to the semi-crystalline carbon matrix.
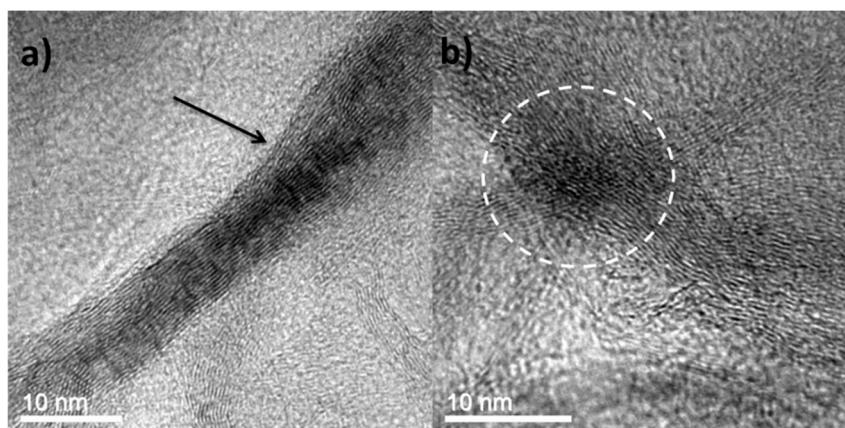

Fig. 10. HRTEM images of turbostratic synthesized carbon black (CB). a) Well-aligned microcrystal of graphite–arrow indicates a Bragg fringe; b) Dotted circle indicating a rotation in stacking plane of graphite micro-crystallites.

3.3 Carbon black structural analysis

The crystalline structure of different conditions was examined via XRD and Raman spectroscopy, as shown in Figs. 11 and 12, respectively. XRD analysis of the carbon nanostructures was conducted to evaluate its structure.
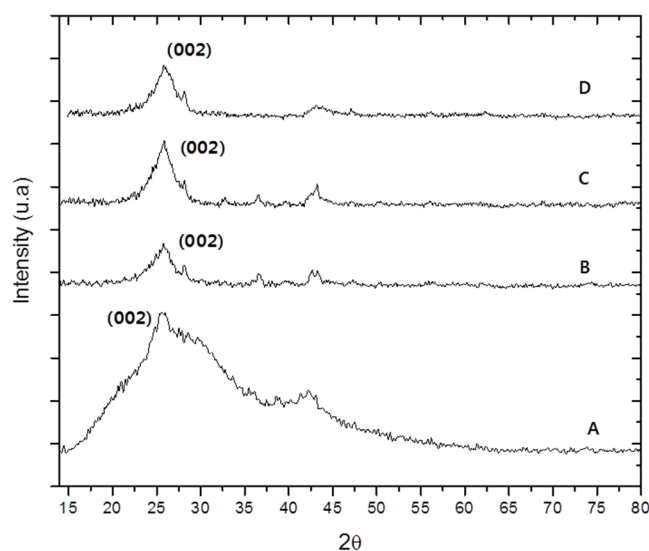

Fig. 11. Carbon black (CB) properties obtained using data from Raman and X-ray diffraction (XRD) techniques.

In Fig. 11, only the (d_{002}) peak appearances in all patterns, 26°, are shown. These diffractograms are typical of turbostratic structures. All samples present the same general structure, as reported in TEM analysis; however, the graphitization degree, related to the inverse of d_{002} distance, changes, as shown in d_{002} distance calculated and presented in Table 2. The higher distance between layers causes the lowest stacking density and a small crystallinity in this direction. The layers are parallel, but their orientation is random in the planes, as shown in HRTEM. The increased propane flow enhanced the samples' graphitization degree (samples C and D), perhaps because of the increased temperature.

Table 2. Carbon black (CB) properties obtained using data from Raman and X-ray diffraction (XRD) techniques.

Sample	I_D/I_G	d_{002} (Å)
A	0.518	3.481
B	0.572	3.468
C	0.514	3.460
D	0.555	3.346

Generally, carbon nanomaterials show intense D and G peaks into 1580 and 1330 cm^{-1}, respectively. These peaks are due to crystallites' growth in size and number, leading to the formation of a partially structured material. Similarly, as shown in Fig. 12, all Raman spectra have these two main peaks. Usually, the peaks around 1330 cm^{-1} relate to disorder and the random orientation in the sample, and the peaks around 1580 cm^{-1} are related to the graphitic nature of carbon material [24].

The higher G band intensity indicates high graphitization/crystallinity. The ratios between the D and G bands (I_D/I_G) measure the amount of disorder in the crystallinity [25, 26]. The values reported for ratio I_D/I_G (Table 2) show that carbon particles have a semi-crystalline structure with a similar disorder degree in all samples. This suggests the existence of a certain amount of amorphous carbon or a low level of graphitization/crystallinity, in agreement with the low intensity in the XRD data.
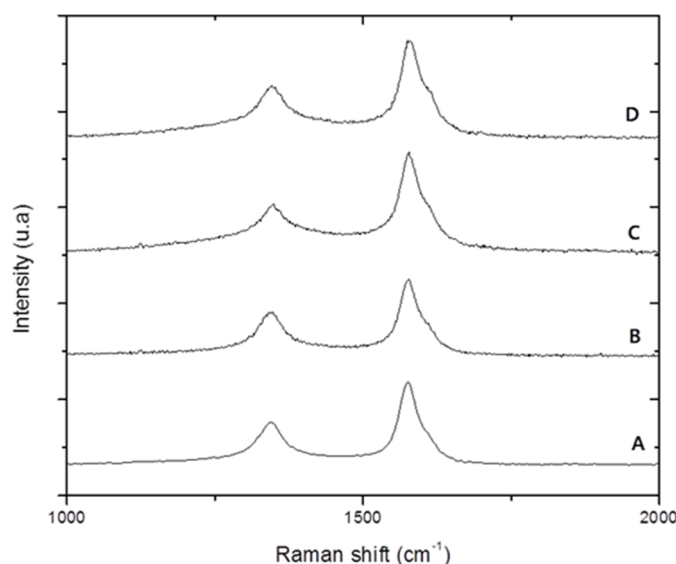

Fig. 12. Raman spectra of carbon black (CB).

3.4 Hypothesis of carbon black particles growth

Knowledge of plasma processes' composition and thermodynamic properties is fundamental in the present study. For this purpose, two methods are widely used: we first considered the Gibbs free energy minimization when several phases were considered, which occurs in low plasma temperature, and the second is based on the law of mass action, where the solution of Saha and Guldberg–Waage laws are considered when only gaseous species are involved (single phase). Knowing species' chemical compositions, the thermodynamic and mass transport properties (enthalpy derivative with respect to temperature and heat capacity at constant pressure) of the gaseous complex mixtures can be calculated, and the first understanding of CB growth can be provided [1, 6, 27–30].

Although soot and CB formation are not processed in equilibrium, this approach offers a possible mechanism associated with propane pyrolysis through plasma. Although several theories have been proposed for carbon particulate formation and growth, there is no overall mechanism that explains the formation of the first nucleus and a post-growth after the first seeds appear. Donnet, Bansal, and Wang [4] proposed reviewing a CB formation mechanism on the basis of pyrolysis and partial oxidation processes. The general mechanism capable of explaining this process is based on three different stages: i) nucleation, which corresponds to the

transformation of the molecular system on the particulate system; ii) aggregation due to collision of particles with size in the order of nanometers; and iii) agglomeration of these particles to form larger ones [4, 6].

An intermediate mechanism between simultaneous polymerization and hydrogenation is more feasible. The more accepted viewpoints are according to the C_2 condensation theory, the acetylene theory, the polyacetylene theory, and the polyaromatization theory, all discussed in [4]. However, each mechanism, by itself, shows shortcomings, so there is no exclusive explanation of the carbon particle growth, but combined theories, as proposed in Bolouri's theory [26], correlate the obtained calculations at the chemical thermodynamic equilibrium (for H/C = 4 and P = 1 bar) with CB growth mechanisms.

3.5 Chemical equilibrium modeling

Calculating the equilibrium composition of the chemical system in the electrode region was modeled using T&TWinner chemical equilibrium software [16, 17], which is based on the method of Gibbs free energy minimization. The thermodynamic and transport properties, which are essential for advanced simulations, can also be calculated. All calculations were based on local temperature and pressure inputs, with temperature ranging from 400 to 8000 K. To examine a scenario of propane pyrolysis in the RGA reactor, a total of 30 species were considered, including electrons, ions, radicals, neutral species, and atomic species. All species were selected according to the literature about the CB process and propane pyrolysis to understand the possible mechanisms. We focused closely on the first nuclei formation to start aggregation and agglomeration of soot, and CB growth [4, 6, 30, 31] was considered as the first approximation of the local thermodynamic equilibrium.

The chemical equilibrium composition calculated from propane as the carbon precursor is shown in Fig. 13. In each cycle, the physics and chemistry parameters change rapidly and drastically within the RGA. High temperature gradients and electromagnetic fields cause carbon particles' growth, not by a particular mechanism but by combining the processes as above described. The population of ionic species occurs with significant densities only at high temperatures, where collisions between ions and molecules are more pronounced, indicating an influence of the ions in the beginning of particle growth.
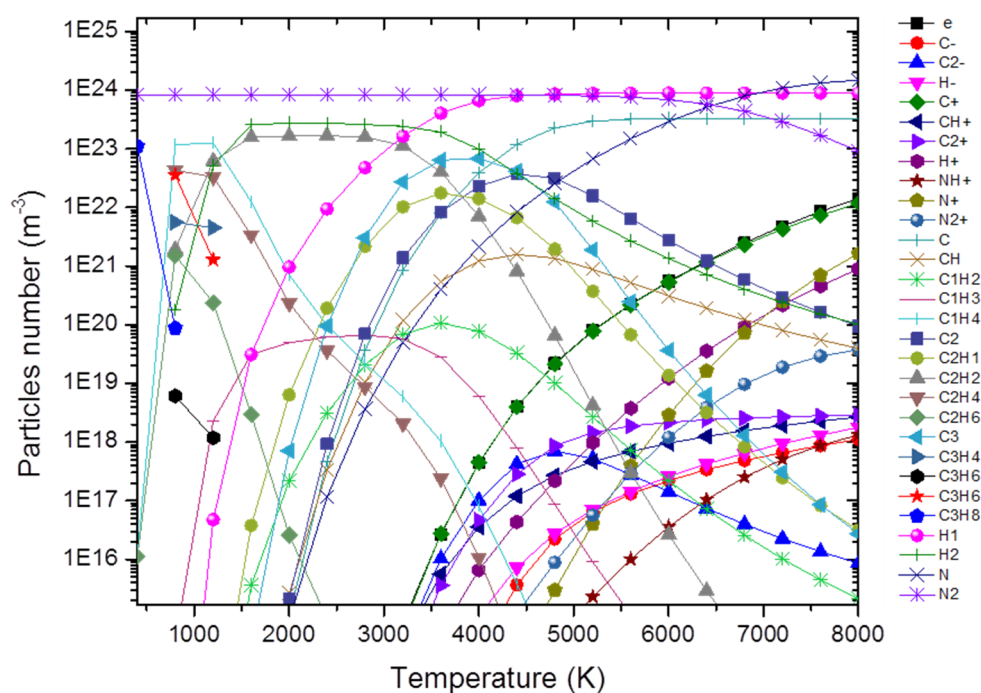

Fig. 13. Thermodynamic equilibrium calculation for propane–N_2 pyrolysis, (P = 1 atm) as a function of temperature, using T&TWinner with constant flow rates: N_2 of 25 L·min^{-1} and C_3H_8 2 L·min^{-1}.

Mass spectroscopy analysis shows that ions rearrange very rapidly into more polynuclear or aromatic structures, which are precursors for CB formation [4]. This situation probably occurs in high temperature regions and consequently high current as shown in zone 2 in Fig. 2 (b), perhaps nucleation region. After this region (zone 1 in Fig. 2 (b)), temperature decreases, and the contribution of carbon growth are due to

polyacetylene theory, as described in [4]. At this moment, particles grow by the abstraction of hydrogen, and the addition of acetylene in the edges, as shown in the dotted circle in Fig. 10 (b), highlights a possible edge of growth. Evidently, acetylene molecules have their maximum production at a temperature range of 1000 to 4000 K.

In a gliding arc reactor, the temperature range in zone 1, shown in Fig. 2 (b), where the discharge transition occurs is the transition region between nucleation and aggregation. [21] Some hydrocarbons are produced at low-temperature regions and can be associated with soot formation instead of CB. Most of the radicals are produced and consumed very fast. However, C_2H and C_2 have a significant amount in the temperature range of 2000–6000 K, and both can be associated with the nucleation and aggregation stages. C_2 condensation theory is essential at high temperatures, whereas C_2H is important at intermediate temperatures [4, 6]; hence, they may be connected in two stages simultaneously. In zone 3 (Fig. 2(b)), the expansion of gas and the decrease of temperature cause a free growth of carbon particle in which particles grow and deposit in the chamber wall.

3.6 Fluid dynamics modeling

The nitrogen velocity profile within the RGA plasma reactor with the velocity peak profile obtained at the swirling zone and homogeneous flow at the electrode region is shown in Fig. 14 (a). Pressure oscillations in a cross-section at the electrode tip, which is favorable for operating RGA reactors are shown in Fig. 14 (b). The velocity profile in a cross-section at the electrode tip with the gas flow concentrated around the electrode, leading to ideal conditions for RGA discharge regime, is shown in Fig. 14 (c).
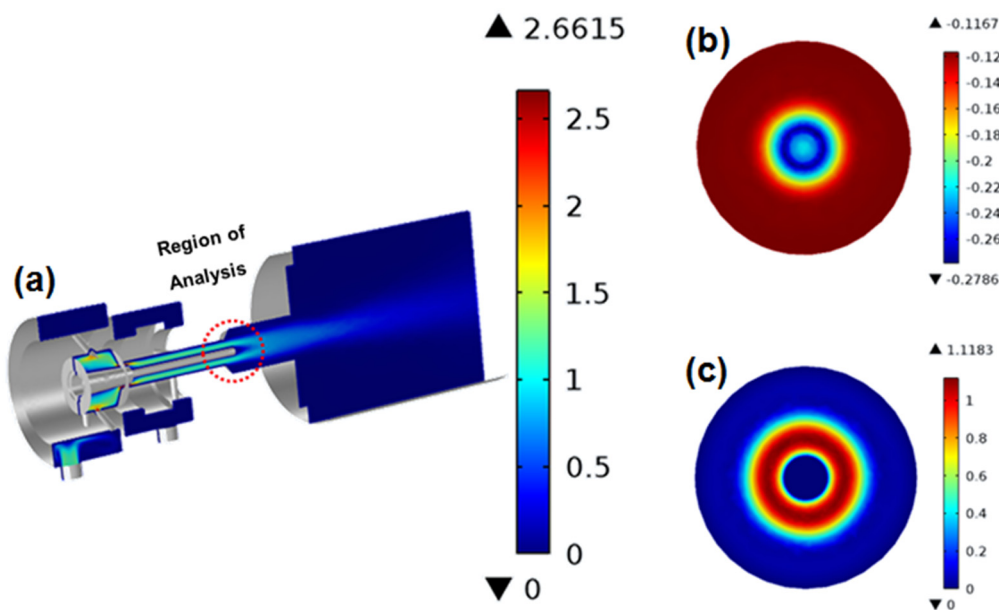

Fig. 14. Fluid dynamics in the RGA reactor: (a) gas velocity profile $(m \cdot s^{-1})$ at a single plane of the 3-D domain, (b) pressure distribution contour (Pa) at the electrode tip, and (c) velocity profile $(m \cdot s^{-1})$ at the electrode tip.

3.7 Electrostatics modeling

The non-uniform electric field at the electrode region is shown in Fig. 15. Three different geometries were examined. Regions with high electric field strengths are favorable for electron emission and discharge ignition. This condition is maximized in the configuration shown in Fig. 15 (a), where the electric field is non-uniform. Rounded electrode tips lead to an increased electron distribution area and a consequent minimization of the electrical field gradients. Therefore, a higher power input is essential to ignite the electric arc when the configuration shown in Fig. 15 (b) was applied.

The obtained results shown in Fig. 15 are aligned with experimental observations at similar conditions, as shown in Fig. 3 [13]. A higher degree of carbon deposition at the electrode tip, as in Fig. 3, implies that a higher reaction rate occurs at this region, which is due to the high electric field strength.
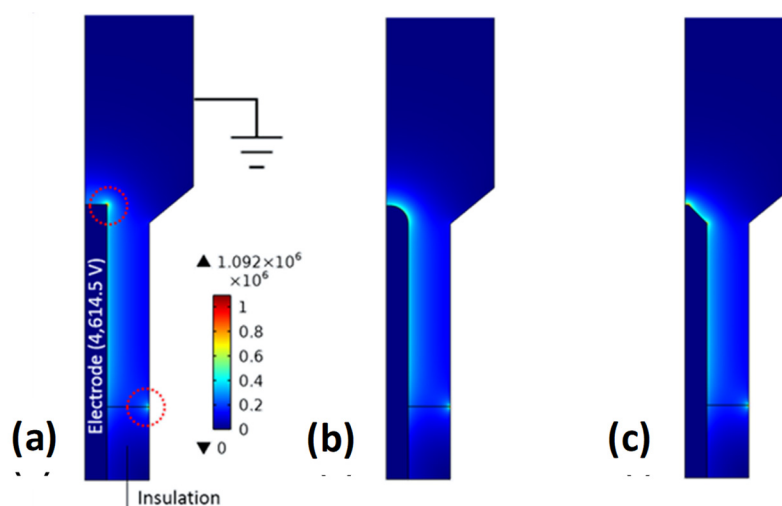
Fig. 15. Electrostatics at the electrode: contours of electric field norm (Vm^{-1}) considering:
(a) rectangular, (b) rounded, and (c) pointed tip topologies.

4. Conclusion

In this work, CB was produced from propane pyrolysis by a non-thermal plasma reactor via rotational gliding arc RGA regime using AC high-voltage and a low current power supplier at atmospheric pressure. The CB particle structure identified was a turbostratic type with small particles fused and graphitic layers randomly formed.

The fluid dynamics, pressure, and velocity profiles, as well as electrostatic properties, electric field strength at the electrode area of the RGA reactor were obtained via COMSOL$^{®}$ Multiphysics software. The chemical composition profile of the RGA reactor in ideal working conditions was estimated via T&TWinner software based on the method of Gibbs free energy minimization method.

The multi-step modeling calculation and the experimental results show that the rate of degradation of propane is high at the electrode tip, which shows a direct relationship with the intensity of the electric field. The multi-step modeling calculation showed to be a strong tool for an RGA reactor design for efficiency achievement.

Acknowledgments

References

[1]   Fabry, F., Flamant, G., and Fulcheri, L., Carbon black processing by thermal plasma. Analysis of the particle formation mechanism. *Chem. Eng. Sci*., Vol. 56 (6), pp. 2123–2132, 2001.
[2]   Baldissarelli, V. Z., Benetoli, L. O. B., Cassini, F. A., Souza, I. G., and Debacher, N. A., Plasma-Assisted Production of Carbon Black and Carbon Nanotubes from Methane by Thermal Plasma Reform., *J. Braz. Chem. Soc*., Vol. 25 (1), 2014.
[3]   Pierson, H. O., Handbook of carbon, graphite, diamond and fullerenes–Properties, processing and applications, Noyes Publications, New Jersey, 1993.
[4]   Donnet, J-B., Bansal, R. C., and Wang, M-J., Carbon black: Science and technology. 2nd. CRC Press, 1993.
[5]   International Carbon Black Association, Carbon Black User's Guide–Safety, Health and Environmental Information. Available from: www.carbon-black.org, 2020.
[6]   Moreno-Couranjou, M., Monthioux, M., Gonzalezaguilar, J., and Fulcheri, L., A non-thermal plasma process for the gas phase synthesis of carbon nanoparticles. *Carbon*, Vol. 47 (10), pp. 2310-2321, 2009.
[7]   Roth, J. R., Industrial Plasma Engineering: Principles. London: Institute of Physics Publishing, 1995.

[8]   Zhukov, M. F., and Zasypkin, I. M., Thermal Plasma Torches: Design, Characteristics, Applications. Cambridge: Cambridge International Science Publishing Ltd, 2007.

[9]   Fauchais, P., and Vardelle, A., Thermal Plasma, *IEEE Trans. Plasma Sci*., Vol. 25 (6), pp. 1258-1280, 1997.

[10] Kim, K. S., Seo, J. H., Nam, J. S., Ju, W. T., and Hong, S. H., Production of hydrogen and carbon black by methane decomposition using DC-RF hybrid thermal plasmas, *IEEE Trans. Plasma Sci*., Vol. 33 (2), pp. 813–823, 2005.

[11] Liu, X. Y., Hong, R. Y., Feng, W. G., and Badami, D., Synthesis of structure controlled carbon nanomaterials by AC arc plasma process, *Powder Tech*., Vol. 256, pp. 158-165, 2014.

[12] Yuan, J. J., Hong, R. Y., Wang, Y. Q., and Feng, W. G., Low-temperature plasma preparation and application of carbon black nanoparticles, *Chem. Eng. J*., Vol. 253, pp. 107-120, 2014.

[13] Liu, J-L., Park, H.W., Chung, W.J., and Park, D-W., High-efficiency conversion of CO_2 in AC-pulsed tornado gliding Arc plasma, *Plasma Chem. Plasma Process*., Vol. 36, pp. 437-449, 2016.

[14] Zhang, H., Du, C., Wu, A., Bo, Z., Yan, J., and Li, X., Rotating gliding arc assisted methane decomposition in nitrogen for hydrogen production, *Int. J. Hyd. Energy*, Vol. 39 (24), pp. 12620-12635, 2014.

[15] Wang, W., Mei, D., Tu, X., and Bogaerts, A., Gliding arc plasma for CO_2 conversion: Better insights by a combined experimental and modelling approach, *Chem. Eng. J*., Vol. 330, pp. 11-25, 2017.

[16] Pateyron, B., Delluc, G., and Fauchais. P., Chemical and transport properties of carbon-oxygen hydrogen plasmas in isochoric conditions, *Plasma Chem. Plasma Process*., Vol. 25, pp. 485-502, 2005.

[17] Tsang, W., Chemical kinetic database for combustion chemistry. Part 3. propane, *J. Phys. Chem. Ref. Data*, Vol. 17 (2), pp. 887-951, 1988.

[18] Elagin, I., Samusenko, A., and Chirkov, A. V., Numerical study of the needle inclination angle effect on the ionic wind direction, *Int. J. Plasma Environ. Sci. Technol*., Vol. 14 (1), pp. e01006, 2020.

[19] Gordon, S., and Mcbride, B. J., Computer program for calculation of complex chemical equilibrium compositions and applications. Cleveland: National Aeronautics and Space Administration (NASA), 1994.

[20] Zhao, T-L., Liu, J-L., Li, G-S., Liu, G-B., Song, Y-H., Xu, Y., and Zhua, A-M., Temporal evolution characteristics of an annular-mode gliding arc discharge in a vortex flow, *Phys. Plasmas*, Vol. 21 (5), pp. 053507, 2014.

[21] Fridman, A., Nester, S., Kennedy, L. A., Saveliev, A., and Mutaf-Yardimci, O., Gliding arc gas discharge, *Prog. Energy Combust. Sci*., Vol. 25, pp. 211-231, 1999.

[22] Pristavita, R., Mendoza-Gonzalez, N-Y., Meunier, J-L., and Berk, D., Carbon blacks produced by thermal plasma: The influence of the reactor geometry on the product morphology, *Plasma Chem. Plasma Process*., Vol. 30 (2), pp. 267-279, 2010.

[23] Aomoa, N., Bhuyan, H, Cabrera, A. L., Favre, M., Diazdroguett, D. E., Rojas, S., Ferrari, P., Srivastava, D. N., and Kakati, M., Rapid synthesis of carbon nanoparticles with an optimized combination of specific surface area and crystallinity by a plasma-assisted single-step process, *J. Phys. D: App. Phys*., Vol. 46 (16), pp. 165501, 2013.

[24] Tuinstra, F., and Koenig, J. L., Raman spectrum of graphite, *J. Chem. Phys*., Vol. 53, pp. 1126–1129, 1970.

[25] Jorio, A., Ferreira, E. H. M., Cançado, L. G., Achete, C. A., and Capaz, R. B., Measuring disorder in graphene with raman spectroscopy, physics and applications of graphene - Experiments, Sergey Mikhailov (Ed.), ISBN: 978-953-307-217-3, InTech, Available from: http://www.intechopen.com/books/physics-and-applications-of-graphene-experiments. 2011.

[26] Bolouri, K. S., and Amouroux, J., Analyse des processus de formation de noir de carbone: Une correlation entre le mecanisme de formation du noir de carbone et les calculs desequilibres chimiques hydrogene-carbone, *Bull. Soc. Chim. Fr*., Vol. 5-6, pp. 101-109, 1983.

[27] Boulos, M. I., Fauchai, S. P., and Pfender, E., Thermal plasmas: Fundamentals and applications. Plenum, New York, 1994.

[28] Andre, P., Abbaoui, M., Bessege, R., and Lefort, A., Comparison between Gibbs free energy minimization and mass action law for a multitemperature plasma with application to nitrogen, *Plasma Chem. Plasma Process.*, Vol. 17 (2), pp. 207-217, 1997.

[29] Wang, W. Z., Murphy, A. B.; Yan, J. D., Rong, M. Z., Spencer, J. W., and Fang, M. T. C., Thermophysical properties of high-temperature reacting mixtures of carbon and water in the range 400-30,000 K and 0.1-10 atm. Part 1: Equilibrium composition and thermodynamic properties, *Plasma Chem. Plasma Process*, Vol. 32, pp. 75-96, 2012.

[30] Renjun, Z., Qiangkun, L., and Zhiyong, L., Study of kinetic models for the reaction of propane, *J. Anal. Appl. Pyrol*., Vol. 13, pp. 183-190, 1988.

[31] Volkan, A. G., and April, G. C., Survey of propane pyrolysis literature, *Ind. Eng. Chem., Process Des. Dev*., Vol. 16 (4), pp. 429-435, 1977.